AgBr photophysics from optical studies of quantum confined crystals

A. P. Marchetti
Imaging Research Laboratories, Eastman Kodak Company, Rochester, New York 14652-3208 and Center for Photoinduced Charge Transfer, University of Rochester, Rochester, New York 14627

K. P. Johansson
Imaging Research Laboratories, Eastman Kodak Company, Rochester, New York 14652-3208

G. L. McLendon
Department of Chemistry and Center for Photoinduced Transfer, University of Rochester, Rochester, New York 14627

(Received 13 August 1992)

Luminescence spectroscopy of nanocrystals (<100 nm) has been used to probe the details of the low-temperature photophysics of AgBr, an indirect-gap semiconductor. Small crystallite size, moderate excitation levels, and radiative decay rates create a situation in which only one electron-hole pair exists in a given nanocrystal. These restrictions eliminate some of the decay channels and simplify the exciton emission spectrum for ≈ 50-nm edge-length crystals. The exciton recombination in 10-nm-diam crystals dominates the emission spectrum. This emission is $>10^4$ times as intense as exciton emission from a macroscopic crystal. Symmetry relaxation, carrier confinement, and impurity exclusion explain this increase in exciton emission. Doping experiments confirm the assignment of one set of exciton lines (BX_8) as recombination emission from an exciton bound to an ionized donor.

I. INTRODUCTION

The behavior of charge carriers, generated by band-to-band excitation, in a material which has undergone a "change in environment" can provide insight into the fundamental properties of the material. Recent experiments on the effect of size restriction on semiconductors have been useful in this respect. Size restriction, that is, forming materials whose physical size is of the same order of magnitude as the "effective electron size" or the exciton radius, can alter selection rules, change photophysical processes, and enhance the importance of such species as surface states.[1-5]

It was shown almost a decade ago that very small crystallites of several different semiconductors (mostly II-VI materials) undergo changes in their optical properties (i.e., absorption and emission characteristics) as their size is reduced, usually to less than 100 nm in diameter. The new energy-level structure had contributions from carrier confinement as well as surface related states. The optical-absorption spectra were more structured than the bulk semiconductors.[3,4] This type of behavior has also been observed in structured semiconductors, such as quantum wells, quantum wires, and quantum dots.[6,7] The behavior of individual charge carries has been treated by a model effective mass, particle-in-a-box Hamiltonian.[8,9] The energy (band-gap) of the lowest $1s$-$1s$ transition as a function of r, the crystallite radius, is given by

$$E(r)=E_g+\frac{h^2\pi^2}{2r^2}\left[\frac{1}{m_e^*}+\frac{1}{m_h^*}\right]-\frac{1.8e^2}{\varepsilon r}+\mathcal{T}_{\rm pol}\ , \qquad (1)$$

where E_g is the band-gap energy of the bulk material, m_e^* and m_h^* are the effective masses of the electron and hole, respectively, e and h have their usual meaning, ε is the static dielectric constant of the material, and $\mathcal{T}_{\rm pol}$ represents polarization terms. This equation can be used to qualitatively predict the magnitude of the shift in the band edge to higher energies as the particle size decreases.[10]

The effect of size restriction on the photophysical properties of indirect-gap materials is less clear. While similar shifts of the band-edge transitions to higher energies might be expected, the effect of confinement may serve to change the nature of the (momentum) forbidden lowest energy transition. It may become "allowed," as the interruption of symmetry at the crystallite surface (which becomes increasingly important as the size of the crystallite decreases) causes a breakdown of the infinite crystal approximation. The effect of size restriction on the electronic properties of the silver halides has been observed as early as 1967, when it was noted that there was a shift to higher energies in the exciton absorption for silver iodide crystallites whose diameters were less than 30 nm.[11] The effect of size restriction on the properties of indirect-gap silver halides was postulated to mix surface electronic states into the crystallite wave function, making the lowest energy indirect-gap transition more "allowed."[3] The breakdown of the infinite crystal approximation has been observed in the small particles (10 nm diameter) of AgBr made in inverted micelles where the "forbidden" indirect exciton transition becomes the primary pathway for luminescent recombination, at low temperatures.[12,13] This emission has a quantum yield of 0.075 ± 0.015, which is at least four orders of magnitude greater than in the bulk.[14]

The indirect transition in silver bromide crystals has been extensively studied.[15-17] The exciton emission,

which in bulk AgBr appears as a set of narrow lines centered around 463 nm (2.63 eV), is visible only at very high experimental sensitivities due to the forbidden nature of the indirect transition. The individual lines have been assigned to the recombination of free excitons (FE's) with phonon involvement. The zero-phonon line of the free exciton is extremely weak. Excitons can also be shallowly trapped at donors or ionized donors. The emission spectrum from weakly bound excitons (BX_n) is shifted to energies below the free indirect exciton emission by an amount equal to the binding energy of the exciton to the donor or ionized donor.[16]

The major pathways for a radiative recombination in bulk AgBr crystals are iodide (impurity) bound exciton emission and donor-acceptor emission.[18–20] The iodide bound exciton (IBE) emits at a peak energy of 2.50 eV (495 nm), with the individual phonon transitions easily resolvable when the spectrum is measured at low temperature ($\approx$6 K). This exciton emission intensity is dependent on the iodide concentration.[21] It has been shown that very small crystals of silver bromide exhibit impurity exclusion effects.[12,13] Nanocrystals have a small spatial extent and therefore a limited number of constituent atoms. When they form, a large fraction of them do not contain impurities. In particular, the emission spectrum from 10-nm-diam spheres of AgBr has almost no contribution from the iodide bound exciton. This occurs because iodide ions, which are ubiquitous in AgBr at about 1 mppm, are found in only one particle in a hundred. The incorporation of the iodide impurities should follow Poisson statistics.

The presence of donor-acceptor recombination at 580 nm, however, does not show a marked size dependence. This band is thought to be due to donor-acceptor recombination, that is, a variety of defect sites that trap electrons and holes separately, which then recombine through tunneling processes. This conclusion is supported by both spectroscopic and magnetic resonance evidence.[19] Interestingly enough, the presence of these trap states does not seem to be significantly affected by size restriction. This suggests that, at least in some large proportion of the crystallites, these charge-carrier traps are "intrinsic" in nature or ubiquitous.

Another restriction imposed by particle size is that of "low carrier density" for a given excitation level. That is, decay pathways that require the products of more than one absorbed photon (exciton, e^- and h^+ pair) to decay will be closed. This condition is normally met using modest energy excitation conditions. A 50-nm edge-length cube of AgBr contains 2.6×10^6 AgBr pairs. The gelatin dispersions (see below) of these microscrystals have a particle density of 1.2×10^{14} cm^{-3} and the interaction volume of the laser beam is estimated to be 10^{-2} cm^3. A 10-mW laser at 325 nm has a flux of 1.6×10^{16} photons/s. Estimating that about a third of the incident light is absorbed by the AgBr leads to an electron-hole pair production per microcrystal of 4.5 pairs/ms. Since the lifetime of the iodide bound exciton is 16 μs (Ref. 20) and the approximate lifetime of the donor-acceptor recombination is 100 μs,[19] we can conclude that even in 50-nm edge-length crystals, most have only one electron-hole pair or exciton at a time. Because the photophysics of size restricted AgBr is confined to this case, biexciton, multiple charge carrier interactions and donor bound excitons will be absent. Donor bound excitons will, of course, be absent because ionized donors such as divalent cation impurities require an additional electron for neutralization. This simplifies the treatment of the electron and hole dynamics.

The intent of our investigation is to add to the understanding of the low-temperature photophysics of the silver halides. Size restriction can be used as a tool to gain more insight into the role that various processes such as thermalization play and into the involvement of the surface in the decay processes.

II. EXPERIMENT

A. Preparation of size restricted silver bromide

Size restricted silver bromide crystals were made using the method of reverse micelles (RMC). This procedure has been detailed elsewhere.[12,14] Silver bromide crystallites were also prepared as photographic "emulsions" (hereafter called "gelatin-stabilized crystallites" or gelatin preparations). The method of gelatin preparation has been detailed elsewhere.[14] Crystals were also grown in polyvinyl alcohol (PVA) in the same manner as the gelatin preparations.

The sizes and morphology of these crystallites was determined by either scanning electron microscopy (SEM), in the case of the largest crystallites, and by transmission electron microscopy (TEM) in the case of the smallest. A variant of TEM, direct lattice resolution was used to examine the lattice spacing of some of the AgBr crystallites.[22] The size of the crystallites in the micelle preparation ranged from 5 to 25 nm in spherical diameter. Sizing of one particular preparation gave an arithmetic mean diameter of 10 nm with a standard deviation of 4 nm. There seemed to be, however, two groups of crystallites, one with a diameter of $\approx$6 nm and the other with a diameter of $\approx$10 nm with some larger crystallites. The crystallites prepared in gelatin were generally cubic in shape and could be made in various sizes from 120 nm down to 40 nm in edge length. A larger sized preparation was fairly monodispersed with a mean cubic edge length of 120 ± 13 nm. A smaller gelatin preparation has a mean cubic edge length of 94 ± 21 nm. The smallest gelatin preparation contained more "rounded' cubes and had a mean edge length of 41 ± 7 nm. The largest PVA preparation had a mean cubic edge length of 55 ± 10 nm. A smaller PVA preparation had crystallites that were very irregular in shape with a mean size 27 ± 10 nm but there were a number of particles that were twice the mean size. The micelle, gelatin, and PVA preparation were easily repeatable, reproducing the grain size and morphology for a given set of conditions.

An electron micrograph using direct lattice resolution techniques[22] is shown for the 55-nm PVA preparation in Fig. 1. The crystallites were examined via lattice imaging to verify that these particles were crystalline in nature. The PVA-stabilized silver bromide particles were found

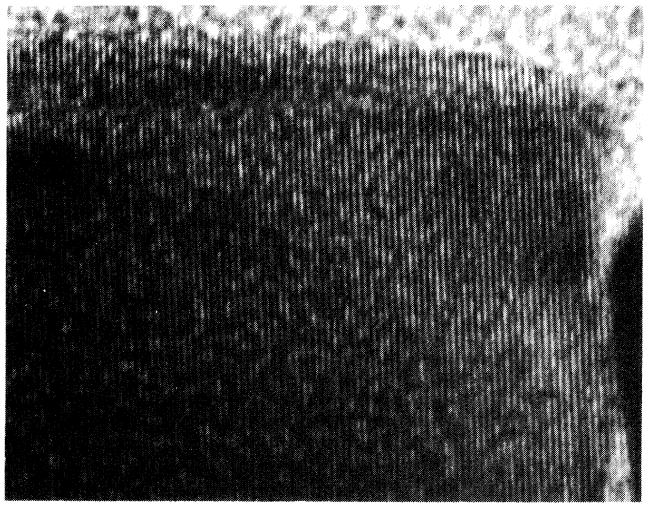

FIG. 1. An electron micrograph using direct lattice resolution techniques of a microcrystal from 55-nm PVA preparation. The magnification is 1.5×10^6. The image is of a (100) plane.

to be crystalline and have lattice parameters that agreed to within 1% with the reported lattice parameters for bulk silver bromide for sizes down to 20 nm (cubic edge length).

B. Low-temperature luminescence apparatus

The low-temperature luminescence spectra were measured using the 325 or 441 nm line of a cw He/Cd laser ($\approx$10 mW) as an excitation source. These lines excite AgBr with an excess energy of about 1.0 or 0.1 eV, respectively. The laser impinged on a sample that was placed in a temperature controlled liquid-helium cryostat. The temperature of the sample could be varied from 1.8 K (pumped He) to room temperature. A typical temperature for luminescence studies was 6 K, although many of the high-resolution spectra were also recorded at 1.9 K.

The fluorescence from the sample was mechanically chopped and resolved with a 1-m spectrophotometer and detected with a red-sensitive photomultiplier tube (PMT). The PMT output was fed into a lock-in amplifier. The lock-in signal was directed into a computer for display and analysis.

C. Time-resolved emission apparatus

Time-resolved emission spectra were obtained on two separate systems.

System 1. Fluorescence lifetimes were measured below the λ point of liquid helium (<2.2 K) on a single photon counting apparatus. Excitation pulses were generated by a home-build cw pumped mode locked neodymium-doped yttrium aluminum garnet (Nd:YAG) laser operating at 76 MHz, which pumped a Coherent 7002-1 cavity dumped dye laser operating with Stryrel-9 laser dye. The output of the dye laser was doubled by focusing the laser beam through an oriented $LiIO_3$ crystal. The doubled dye laser output had a wavelength of approximately 405 nm, with a pulse duration of 10 ps. The excitation beam was collinear with the emission signal, and was separated from the emission by the placement of an interference filter of the desired emission wavelength after the sample. Emission light was focused into a 0.25-m Spex monochromater with a 600 lines/mm grating. The resolved emission was detected by a Hamamatsu R2809-11 MCP-PMT. The MCP output was passed through two inverting amplifiers whose output was then channeled through a Tennelec constant fraction discriminator (CFD). The output of the constant fraction discriminator was sent to the start channel of a time-to-amplitude converter. A small fraction (0.25%) of the dye laser light was incident on a reference photodiode, whose signal was sent to the CFD and subsequently to an electronic delay line. This delayed reference pulse was then sent to the stop channel of the time-to-amplitude converter. The time-to-amplitude converter output was sent to a multichannel analyzer-computer. System response time was approximately 50 ps. The time per channel was approximately 10 ps (4096 channels). The sample was cooled in a Janis liquid-helium optical cryostat, and spectra were taken.

System 2. Time resolved emission spectra were also collected on a system using the pulses from a pulsed N_2 laser as the exciting light, with a pulse duration of approximately 500 ps and an energy of about 3–5 mJ/pulse. The excitation was at 90° relative to the emission collection optics. The emission was focused into a 1-m spectrometer, and detected with a cooled photomultiplier. The photomultiplier response was fed into a programmable amplifier plug-in on a Tektronix 7912 AD digitizer through a 50 Ω terminator. The decay curves are the result of at least 64 averages. The digitizer was externally triggered by the output of a fast photodiode that detected a small fraction of the excitation pulse from the nitrogen laser. Data acquisition, display, and analysis was computerized. The temporal resolution of this system was 7 ns. The sample was cooled in a helium cryostat, with a temperature controller. Temperatures could be varied between 5 and 300 K. Temperatures below 4.2 K were obtained by using a mechanical pump to lower the pressure in the liquid-helium filled sample chamber to below the critical point.

III. RESULTS

The visible emission spectra from a 10-nm-diam, a 41-nm cubic edge length, and a bulk AgBr sample are shown in Fig. 2. These spectra demonstrate the large changes ($>10\,000\times$) engendered in the emission spectra of AgBr by size reduction. The spectrum of the 10-nm crystallites is dominated by the "free" exciton emission which has an estimated quantum yield[14] of 0.075 ± 0.015. This emission spectrum has almost no contribution from iodide bound excitons ($\lambda_{max}=495$ nm). This is a consequence of impurity exclusion.[12]

High resolution spectra, in the region of the free exciton emission, are shown for the 41-nm gelatin preparation, a repeat of the gelatin preparation that was doped

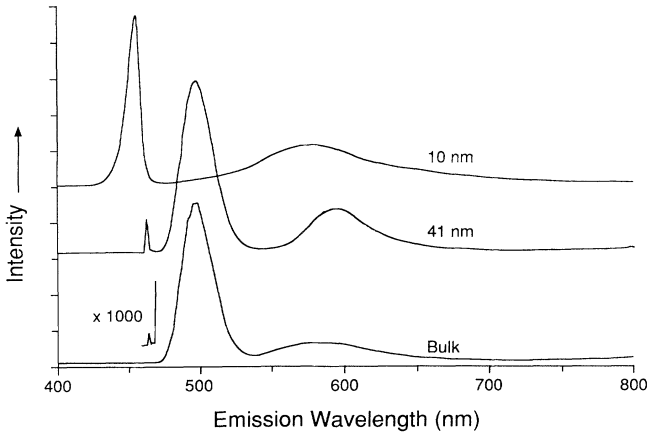

FIG. 2. The steady-state luminescence spectrum of a bulk (3×3 mm) crystal of AgBr, a gelatin preparation containing 41-nm edge-length "rounded" cubes of AgBr, and a reverse micelle preparation containing 10-nm spheres of AgBr. The exciton wavelength was 325 nm and the temperature was less than 6 K. The free exciton emission is found at 463 nm, the iodide bound exciton emission peaks at 495 nm, and the donor-acceptor recombination peaks at about 580 nm.

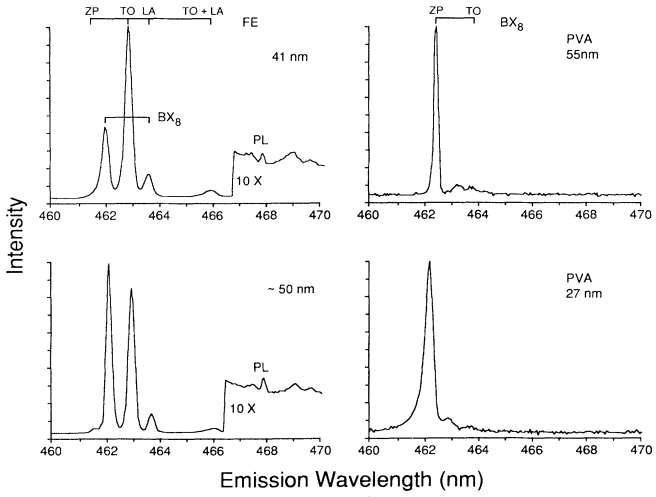

FIG. 3. The steady-state luminescence spectrum of a gelatin preparation containing 41-nm crystallites of AgBr, a gelatin preparation of ≈50-nm crystallites for AgBr doped with 100 mppm formal concentration of Pb^{+2}, a polyvinylalcohol preparation of 55-nm cubic microcrystals of AgBr (see Fig. 1), and a PVA preparation of 27-nm particles in the free exciton region. The excitation was 325 nm and the temperature was less than 6 K. Lines marked PL are plasma lines from the laser and are used for wavelength calibration.

with Pb^{2+} at a formal concentration of 100 mppm, a 55-nm PVA preparation, and 27-nm PVA preparation are shown in Fig. 3. Line positions (vacuum corrected) and assignments for these and other samples are given in Table I. The assignments of the various lines were made by comparison of the line positions of several sizes of crystallites with the known line positions and assignments.[16,23]

The temperature dependence of the free exciton emission intensity has been examined in both the micelle preparations (10 nm) and the gel preparations (50 nm). A plot of the natural logarithm of the inverse intensity versus the inverse of the temperature gives a straight line in the temperature range between 40 and 70 K. This can be interpreted as the exciton ionizing with an activation energy of 30±8 meV for the micelle preparation and 23±6 meV for the 41-nm gelatin preparation. These values agree with estimates from the effective-mass approximation which predicts a binding energy of 28 meV.[25]

Some lifetime measurements have been made on the free exciton emission.[16,24] The bulk crystal measurement were found to be sensitive to sample temperature. The literature data and these measurements are given in Table II.

TABLE I. Line positions (vacuum corrected eV) and assignment of various size restricted AgBr samples. Temperatures were 6 or 1.9 K.

Size/Prep.[a]	ZP_{ex}	$ZP\ BX_8$	TO_{ex}	LA_{ex}, $TO\ BX_8$	Comment
Bulk	2.6838	2.6801	2.6756	2.6717	Refs. 16,23
94/gel		2.6808	2.6763		Δ < 1 meV
55/PVA		2.680	2.675	2.673	Δ < 1 meV
50/gel[b]	2.6850	2.6818	2.6771	2.6731	Δ = 1.5 meV
41/gel	2.6858	2.6823	2.6774	2.6734	Δ = 2.0 meV
27/PVA[c]		2.682	(shaded to higher eneriges)		Δ = 2 meV
10/RMC[c]			2.725		Δ = 49 meV

[a]Mean sizes are in nm and the preparative mediums are indicated.
[b]This preparation contained 100 mppm Pb^{2+}.
[c]The fine structure in the smaller crystallites is lost in the broadening line shape that tails to higher energies. This broadening is due to the effect of size distribution on the emission energies. The peaks are listed as $ZP\ BX_8$ transitions for PVA preparation and TO_{ex} for the reverse micelle preparation because these are the strongest lines in the larger crystallites although they are a convolution of free and bound exciton with photons.

TABLE II. "Free" exciton lifetimes for size restricted crystal of AgBr.

Size	Temperature (K)	Lifetime (ns)	Comments
Bulk	1.7	65±10	Ref. 16
Bulk	<2.2	135±25	Ref. 24
41 nm	1.9	<7	
10 nm	<2.2	3±2	

The effect of size restriction on the emission and phonon structure in the recombination emission from the iodide bound exciton is shown in Fig. 4. Here, in contrast to the free exciton, the emission peaks are shifted to lower energies. The 0-0 and phonon bands are also broadened as the size is reduced. The effect of size restriction on the iodide bound exciton emission lifetime is given in Table III. Here we see that as the size is reduced the single exponential decay of 17 μs that is observed in bulk and "large" crystallites changes into a biexponential decay. As the crystallite size becomes even smaller the faster decay becomes a larger fraction of the emission. The lifetime effects may be due to iodide ions at or near the surface which bind excitons.

The relative intensities of the free exciton emission to the iodide bound exciton emission of a 50-nm gel preparation are shown in Fig. 5 for two excitation wavelengths: 325 and 441 nm; 325 nm excitation provides about 1 eV excess energy ($E_{325}-E_g$), while 441 nm provides only 0.1 eV excess energy. These spectra show that the free exciton emission is stronger relative to the iodide bound exciton when excitation occurs with a large excess energy with band-to-band excitation. A very different ratio will be observed for excitation near the band edge in the exciton absorption region.

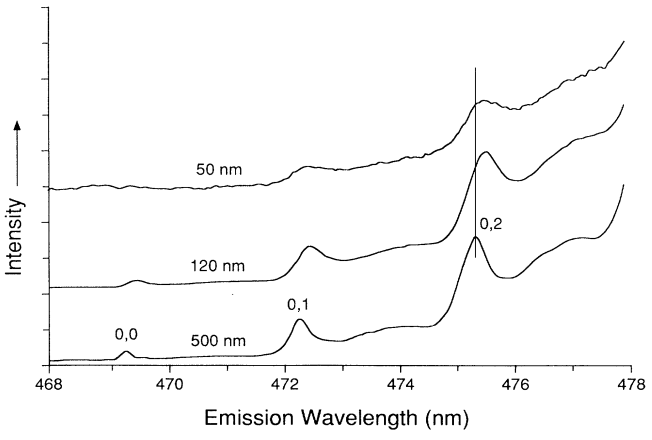

FIG. 4. The emission spectrum of a gelatin preparation of ≈500-nm crystals of AgBr, a gelatin preparation of 120-nm crystals of AgBr, and a gelatin preparation of 50-nm crystals of AgBr in the region of the iodide bound exciton emission. The temperature was less than 6 K and the excitation wavelength was 325 nm. The vertical line at the 0,2 transition emphasizes the shift to lower energies with decreasing particle size.

TABLE III. Lifetime data for iodide bound exciton emission in size restricted AgBr crystallites. Temperatures were less than 6 K.

Size	Lifetime	Comments
Bulk	16±2 μs	Ref. 21
Bulk	16±2	Ref. 24
500 nm	17±2	
100	17±2	
	0.2±0.04	
41	20±3	
	12±3 ns	

IV. DISCUSSION

The free exciton emission in the bulk crystal is an extremely small fraction (<0.0001) of the total emission (see Fig. 2). As the size is reduced so that the average diameter of the crystallites is 10 nm or less this emission becomes the dominant radiative pathway. This dominance occurs for a number of reasons: impurity exclusion, symmetry relaxation, low carrier density and carrier confinement, all related to the reduced size of the crystallites. The impurity exclusion is manifest by the absence of the iodide bound exciton emission.[12,13] The symmetry relaxation is manifest by the reduction in the free exciton emission lifetime as shown in Table II. The free exciton emission lifetime was estimated to be about 10 ns in Ref. 16; the measured value given in Table II is for an exciton bound to an ionized donor. The investigations outlined in Ref. 24 indicate that the free exciton lifetime is greater than 100 ns in annealed crystals. Work on gelatin grown microcrystals suggests that they are less disordered than melt grown crystals and that the appropriate comparison for the size restricted crystals is to the longer lifetimes. The low carrier density effects are indicated in Fig. 3, which shows the high resolution spectra in the region of

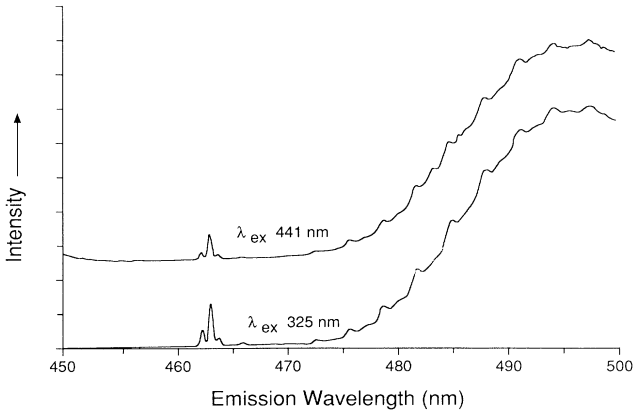

FIG. 5. The emission spectrum of a gelatin preparation containing 50-nm nanocrystals of AgBr at two exciton wavelengths, 325 and 441 nm. The temperature was less than 6 K. Note the larger intensity of the exciton emission at 463 nm in comparison to the iodide bound exciton for excitation at 325 nm.

the free exciton emission. The spectrum from the undoped gel sample (or the PVA sample) exhibits a much simpler structure than that found in bulk samples.[16] In addition, the spectrum of the sample doped with Pb^{2+} is the same as the undoped except for an increase in the intensity of the line at 2.6818 eV. This is in contrast to doped bulk samples which exhibit new lines that are assigned to excitons bound to substitutional $[(Pb^{2+})^-]$ donors.[16] The absence of any donor bound excitons is one manifestation of low carrier density effects. This absence and the increase in intensity of the 2.6818 eV line in the doped sample confirms the assignment of this line as the zero-phonon transition of an ionized donor bound exciton (BX_8).[16]

Carrier confinement effects in AgBr should occur when the electron-hole capture radius becomes a substantial percentage of the crystallite radius. The capture cross section can be estimated by assuming that the capture radius is the distance where the mean thermal energy equals the Coulomb energy or from the Langevin formula[26,27]

$$\sigma = \frac{4\pi e \mu_m}{v\varepsilon} . \tag{2}$$

Using the sum of the microscopic electron and hole mobilities at helium temperatures ($\mu_m = 8$ m^2/V s), the mean velocity for an electron in a parabolic conduction ($v = [8kT/\pi m_p^*]^{1/2} = 2\times 10^4$ m/s at 3 K), the static dielectric constant ($\varepsilon = 10.64$), and the charge on an electron (e), the cross section is estimated to be 6.8×10^5 nm^2.[25] This corresponds to a capture radius of greater than 400 nm. A similar estimate is obtained from calculating the distance at which the thermal energy equals the Coulomb energy.

With the above estimates for the capture cross section at liquid-helium temperatures, the question arises as to why any emission other than the exciton recombination is observed in crystals smaller than 400 nm. The answer should depend on how the electron and hole, created with excess energy, thermalize. If the partition of energy in creating the electron-hole pair and the energy loss were such that one carrier reached thermal velocities before the other, then that carrier would have time to interact with traps with smaller cross sections. Conservation of momentum, using the effective polaron masses for the electron ($m_p^* = 0.2897$) and the hole ($\langle m_p^* \rangle = 1.1$), indicate that the electron carries away almost four times as much energy as the hole.[25] The dominant relaxation method for a hot carrier when the carrier temperature is greater than 30 K should be polar optical scattering.[28] A consideration of the expressions for the rate of energy loss by this process indicates that both electrons and holes thermalize similarly. But the rate of energy loss is directly proportional to the polaron coupling constant (α) which is larger for holes ($\alpha = 2.8$) than for electrons ($\alpha = 1.6$). Thus the electrons start out with almost four times more energy than the holes and they thermalize slower. This offers a plausible explanation for the observation of both iodide bound exciton and donor-acceptor emission in the 50-nm crystallites.

The simple picture, outlined above, suggests that if the electron and hole are created with less excess energy (longer excitation wavelength), then the electron and hole will come to thermal equilibrium concurrently and the proportion of free exciton emission should increase. The opposite effect is shown in Fig. 5. This result suggests that the thermalization process with low excess energy and/or the exciton formation of nearly thermalized carriers is more complex and carrier velocity dependent. Alternately, there may be some other inelastic process occurring when there is sufficient excess energy, that removes a significant fraction of the electron's energy. Such an inelastic process might bring some electrons to thermal energies in the same time frame as the hole.

The high-resolution spectra of the samples prepared in PVA differ significantly from those prepared in gelatin. In the PVA samples, the dominant emission is from BX_8, that is, from free excitons bound to ionized donors. The gelatin prepared samples contain a mixture of free exciton and BX_8 recombination. The PVA preparation must introduce a significant number of ionized donors into the crystallites. At this time it is not know if these ionized donors are cation impurities or interstitial silver ions. This result also suggests that caution should be used in studying PVA preparations as the emission contains little or no contribution from free excitons.

It is known that free exciton emission exhibits an asymmetric line shape due to exciton kinetic energy broadening.[29] This has been observed in bulk AgBr emission.[16,24] This asymmetry is not observed in the free exciton lines shown in Fig. 3. This lack of asymmetry suggests that confined excitons are more rapidly thermalized, due to interaction with the surface.

The observed shifts to higher energies due to size restriction are listed in Table I. Prediction of these shifts for the AgBr exciton line positions as a function of size should not come from Eq. (1) as the temperature dependence of the exciton emission intensity suggests that a more realistic model for this system would be a confined hydrogen atom. The free exciton is often modeled by an effective mass scaled hydrogenic system.[25] A hydrogenic system in the center of a spherical box should be a reasonable model for an exciton in quantum confined semiconductor crystallite as it is known that free excitons avoid surfaces.[30] Variation solutions (as well as exact solutions) have been obtained for the problem of a hydrogen atom in an infinite spherical box.[31]

Using the tabulated data in Ref. 31 and scaling it for an effective-mass exciton in AgBr ($R = R_0\mu_p^*/\varepsilon^2 = 28$ meV and $a = a_0\varepsilon/\mu_p^* = 2.5$ nm where R_0 is the binding energy of a hydrogen atom, a_0 is the Bohr radius, and $1/\mu_p^* = 1/m_e^* + m_h^*$) predicts that the shift for the 41-nm rounded cubes (treated as spheres) should be less than 1 meV and the shift for the 10-nm spheres should be 21 meV. These predictions are in qualitative agreement with the data in Table I, but point out the problem of making such comparisons when the particles are polydispersed in size. This problem is exacerbated by the fact that the exciton emission yield is strongly dependent upon size, as is light absorption. Until monodispersed samples of AgBr are fabricated the use of more complex models is unwarranted.[32]

The effect of size reduction on iodide bound exciton emission, as shown in Fig. 4 and Table III, manifests itself at larger sizes than the effects on the free exciton emission. The 0-0 line and the lines involving various numbers of phonon broaden and shift to lower energies (longer wavelengths) as the size is reduced. The shift is in a direction opposite to that of the free exciton emission. The exponential emission decay of bulk samples is found to become biexpontential (multiexponential?) with the shorter decay component continuing to decrease in apparent lifetime and to become a greater fraction of the emission as the size is reduced.

These effects are due to the fact that iodide segregates, to some extent, to the surface during gelatin growth (and melt growth),[33,34] and that the surface-to-volume ratio is increasing as the size is decreased. The system can be thought of as iodide bound excitons either at the surface, that is, at a distance at which the surface influences the exciton emission, or in the bulk. The bulk excitons decay more or less normally but the surface excitons will decay more rapidly due to symmetry relaxation. The shift to longer wavelengths indicated that the exciton is bound somewhat more strongly by surface iodides. The broadening of the band occurs because, in actuality, there will be a distribution of distances from the surface which influences the exciton.

V. SUMMARY

The generalized radiative decay scheme for AgBr, excited with energies significantly above the band-gap-energy, is given in Fig. 6. Here it is indicated that electrons and holes created by band-to-band excitation must thermalize before they can interact with ionized donors, ionized acceptors, impurities, or each other. The energy partition and thermalization rates are critical in determining how the electron and the hole are trapped and which decay paths are operative. Size restriction simplifies the exciton emission spectrum by eliminating the donor bound exciton recombination. It also modifies the iodide bound exciton emission by emphasizing the role of surface iodide. Size restriction should also modify the donor-acceptor recombination kinetics but to date this has not been observed.

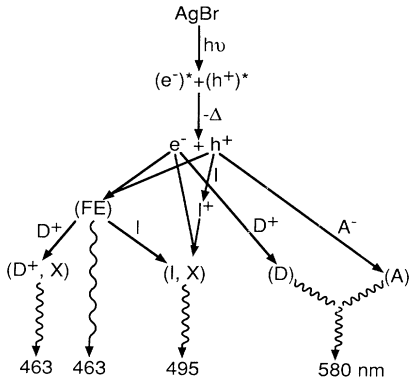

FIG. 6. A schematic of the photophysical processes occurring in size restricted AgBr. As discussed in the text, the relative rates of electron and hole thermalization are important in determining the recombination pathways. Two mechanisms for the formation of iodide bound excitations (I,X) have been postulated but to date their relative contributions have not been determined.

[1]L. E. Brus, J. Chem. Phys. **79**, 5566 (1983).
[2]A. Henglein, Ber. Bunsenges. Phys. Chem. **86**, 301 (1982).
[3]R. Rossetti, S. M. Beek, and L. E. Brus, J. Am. Chem. Soc. **104**, 7322 (1982).
[4]Y. Wang, A. Suna, W. Mahler, and K. Kasowski, J. Chem. Phys. **87**, 7315 (1987).
[5]E. Kartheuser, in *Polarons in Ionic Crystals and Polar Semiconductors,* edited by J. T. Devreese (American Elsevier, New York, 1971).
[6]K. Ploog and G. Dohler, Adv. Phys. **32**, 285 (1983).
[7]D. Heitmann, T. Demel, P. Grambow, M. Kohl, and K. Ploog, in *20th International Conference on the Physics of Semiconductors,* edited by E. M. Anastassakis and J. D. Joannopoulos (World Scientific, Teaneck, NJ, 1990), p. 13, and references cited therein.
[8]M. G. Bawendi, M. L. Steigerwald, and L. E. Brus, Ann. Rev. Phys. Chem. **41**, 477 (1990).
[9]N. Chestnoy, T. D. Harris, and L. E. Brus, J. Phys. Chem. **90**, 3393 (1986).
[10]L. E. Brus, J. Chem. Phys. **80**, 4403 (1984).
[11]C. R. Berry, Phys. Rev. **161**, 848 (1967).
[12]K. P. Johansson, G. L. McLendon, and A. P. Marchetti, Chem. Phys. Lett. **179**, 321 (1991).
[13]H. Kanzaki and Y. Tadekuma, Solid State Commun. **80**, 33 (1991).
[14]K. P. Johansson, A. P. Marchetti, and G. L. McLendon, J. Phys. Chem. **96**, 2873 (1992).
[15]W. von der Osten, Physica **146B**, 240 (1987).
[16]W. von der Osten and H. Stolz, J. Phys. Chem. Solids **51**, 765 (1990).
[17]H. Kanzaki and S. Sakuragi, J. Phys. Soc. Jpn. **29**, 924 (1970).
[18]W. Czaja and A. Baldereschi, J. Phys. C **12**, 405 (1979).
[19]A. P. Marchetti, M. S. Burberry, and J. P. Spoonhower, Phys. Rev. B **43**, 2378 (1991).
[20]S. Sakuragi and H. Kanzaki, Phys. Rev. Lett. **38**, 1302 (1977).
[21]F. Moser and S. Lyu, J. Lumin. **3**, 447 (1971).
[22]P. Hirsch, A. Howie, R. B. Nicholson, D. P. Pashley, and M. J. Whelan, *Electron Microscopy of Thin Crystals* (Krieger, Malabar, FL, 1977), Chap. 15.
[23]W. von der Osten (private communication).
[24]E. Kawate and T. Masumi, J. Phys. Soc. Jpn. **57**, 1814 (1988).
[25]A. P. Marchetti and R. S. Eachus, in *Advances in Photochemistry,* edited by D. Volman, G. Hammond, and D. Neckers (Wiley, New York, 1992), Vol. 17.
[26]P. Langevin, Ann. Chem. Phys. **28**, 433 (1903).
[27]J. F. Hamilton, Adv. Phys. **37**, 359 (1988).
[28]K. Seeger, *Semiconductor Physics* (Springer-Verlag, New York, 1988), Chap. 6.
[29]P. J. Dean and D. C. Herbert, in *Excitons,* edited by K. Cho (Springer-Verlag, New York, 1979), Chap. 3.

[30]S. Satpathy, Phys. Rev. B **28**, 4585 (1983), and references cited therein.
[31]J. L. Marin and S. A. Cruz, Am. J. Phys. **59**, 931 (1991), and references cited therein.
[32]Y. Kayanuma, Phys. Rev. B **38**, 9797 (1988).
[33]B. K. Furman, G. H. Morrison, B. I. Saunders, and Y. T. Tan, J. Appl. Phys. **51**, 5342 (1980).
[34]L. M. Niedzwicki and Y. T. Tan, J. Photogr. Sci. **35**, 155 (1987).

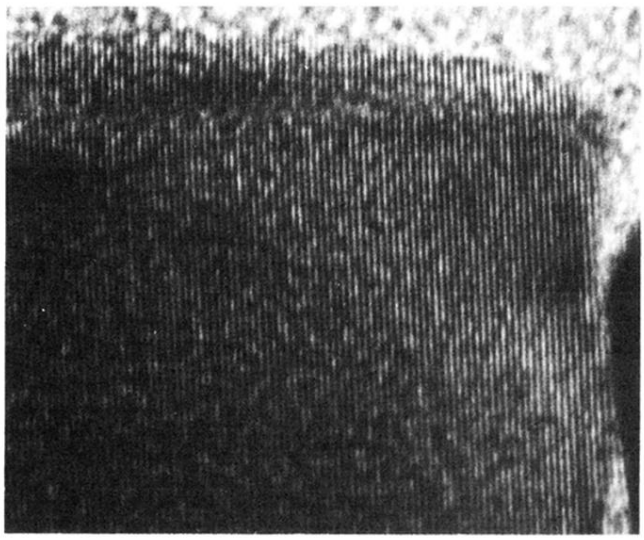

FIG. 1. An electron micrograph using direct lattice resolution techniques of a microcrystal from 55-nm PVA preparation. The magnification is 1.5×10^6. The image is of a (100) plane.